MAGIC: Mosaic Analysis by gRNA-Induced Crossing-over

Sarah E. Allen[1,3], Gabriel T. Koreman[1,2,3], Ankita Sarkar[1,2,3], Bei Wang[1,2], Mariana F. Wolfner[1,4], and Chun Han[1,2,4]

[1]Department of Molecular Biology and Genetics, Cornell University, Ithaca, NY 14853, USA

[2]Weill Institute for Cell and Molecular Biology, Cornell University, Ithaca, NY 14853, USA

[3]These authors contributed equally to this work, listed alphabetically

[4]For correspondence: mariana.wolfner@cornell.edu (MFW) and chun.han@cornell.edu (CH)

Abstract:

Mosaic animals have provided the platform for many fundamental discoveries in developmental biology, cell biology, and other fields. Techniques to produce mosaic animals by mitotic recombination have been extensively developed in *Drosophila melanogaster* but are less common for other laboratory organisms. Here, we report mosaic analysis by gRNA-induced crossing-over (MAGIC), a new technique for generating mosaic animals based on DNA double-strand breaks produced by CRISPR/Cas9. MAGIC efficiently produces mosaic clones in both somatic tissues and the germline of *Drosophila*. Further, by developing a MAGIC toolkit for one chromosome arm, we demonstrate the method's application in characterizing gene function in neural development and in generating fluorescently marked clones in wild-derived *Drosophila* strains. Eliminating the need to introduce recombinase-recognition sites in the genome, this simple and versatile system simplifies mosaic analysis in *Drosophila* and can be applied in any organism that is compatible with CRISPR/Cas9.

Keywords: *MAGIC*, *mosaic analysis, CRISPR/Cas9, gRNA, clonal analysis, germline, imaginal disc, da neurons, Drosophila dominant female sterility,*

25 **Introduction:**

26 Mosaic animals contain genetically distinct populations of cells that have arisen from one zygote.
27 Mosaic animals have historically played important roles in the study of pleiotropic genes, developmental
28 timing, cell lineage, neural wiring, and other complex biological processes. Given its genetic tractability,
29 *Drosophila* has been a major system for generating and studying such mosaics [1], which have led to
30 important discoveries such as developmental compartments [2], cell autonomy [3], and maternal effects
31 of zygotic lethal genes [4]. Mosaic (also called clonal) analysis is currently used to study tumor
32 suppressors [5], signaling pathways [6], sleep-wake behaviors [7], cell fates [8], and neuronal lineages
33 [9], among other biological processes.

34 The earliest mosaic analyses relied on spontaneous mitotic recombination [10], rare events in which
35 a DNA double-strand break (DSB) during the G_2 phase of the cell cycle is repaired by homologous
36 recombination, resulting in the reciprocal exchange of chromosomal arms between homologous
37 chromosomes distal to the site of the DNA crossover (reviewed in Griffin et al., 2014). Ionizing
38 radiation, such as X-rays [12], cause DSBs and thus were later used in *Drosophila* to increase the
39 baseline level of mitotic recombination [13]. However, ionizing radiation breaks genomic DNA at
40 random locations and is associated with a high degree of lethality.

41 To overcome these limitations, the yeast Flippase (Flp)/FRT system was introduced into *Drosophila*
42 to mediate site-specific recombination at FRT sites [14,15], enabling the development of an ever-
43 expanding toolbox with enhanced power and flexibility for clonal analysis [15–19]. This system requires
44 that both homologous chromosomes carry FRT sites at the same position proximal (relative to the
45 centromere) to the gene of interest, and an independent marker on one of the homologs to allow
46 visualization of the genetically distinct clones [15]. For clonal analysis in the *Drosophila* germline, a
47 dominant female sterility (DFS) ovo^{D1} transgene was combined with Flp/FRT methods, allowing
48 production of, and selection for, germline clones homozygous for a mutation of interest in a
49 heterozygous mother [20,21]. In this "Flp-DFS" technique, egg production from ovo^{D1}-containing
50 heterozygous and homozygous germline cells is blocked, resulting in progeny derived exclusively from

germline clones lacking *ovo*^{D1} that were generated by mitotic recombination [22]. Clonal analysis based on somatic recombination has also been achieved in mice using the Cre-LoxP system and the reconstitution of fluorescent protein genes as markers [23,24]. Despite these successes, site-specific recombination systems have not been widely used for mitotic recombination in model animals beyond *Drosophila melanogaster* due to the challenging task of introducing recombinase-recognition sites into centromere-proximal regions for every chromosome.

Given the power of mosaic animals in biological research, it would be useful to have a more general approach for inducing interhomolog mitotic recombination in any organism, circumventing the challenges just mentioned. The CRISPR/Cas9 system has great potential for extending clonal analysis, because it can create targeted DSBs in the genomic DNA of a wide array of organisms [25]. This binary system requires only the Cas9 endonuclease and a guide RNA (gRNA) that specifies the DNA target site [26], both of which can be introduced into the cell independently of the location of the target site. CRISPR/Cas9-induced DSBs can be repaired either by non-homologous end joining (NHEJ) or homology-directed repair (HDR). So far, most CRISPR/Cas9 applications in animals have been focused on NHEJ-mediated mutagenesis and HDR-mediated gene replacement [27]. Recently, several studies demonstrated that CRISPR/Cas9-induced DSBs can also induce targeted mitotic recombination in yeast and in the germlines of *Drosophila*, houseflies, and tomatoes [28–31], suggesting the possibility of exploiting this property of CRISPR/Cas9 for mosaic analysis. Here, we report mosaic analysis by gRNA-induced crossing-over (MAGIC), a novel technique for mosaic analysis based on CRISPR/Cas9. This method can be used to generate mosaic clones in both the *Drosophila* soma and germline. Based on this method, we built a convenient toolkit to generate and label mosaic clones for genes located on chromosome arm 2L. We demonstrate the success of our toolkit for clonal analysis in the soma and the germline and show its applications in analyzing gene functions in neuronal dendrite development. Lastly, we also demonstrate that MAGIC can be used successfully with unmarked wild-derived strains, indicating that this method can be extended to organisms beyond *Drosophila*.

Results:

77 ***Rationale for MAGIC***

78 MAGIC relies on the action of gRNA/Cas9 in a proliferating cell during G_2 phase to generate a DSB at a
79 specific position on one chromatid of a homologous pair (Figure 1A). The DSB can induce a crossover
80 between this chromatid and a chromatid from the homologous chromosome, resulting in exchange of
81 chromosome segments between the two chromatids at the location of the DSB. During the subsequent
82 mitotic segregation of chromosomes, a 50% chance exists for identical distal chromosome segments to
83 sort into the same daughter cells, generating "twin spots", which contain two genetically distinct

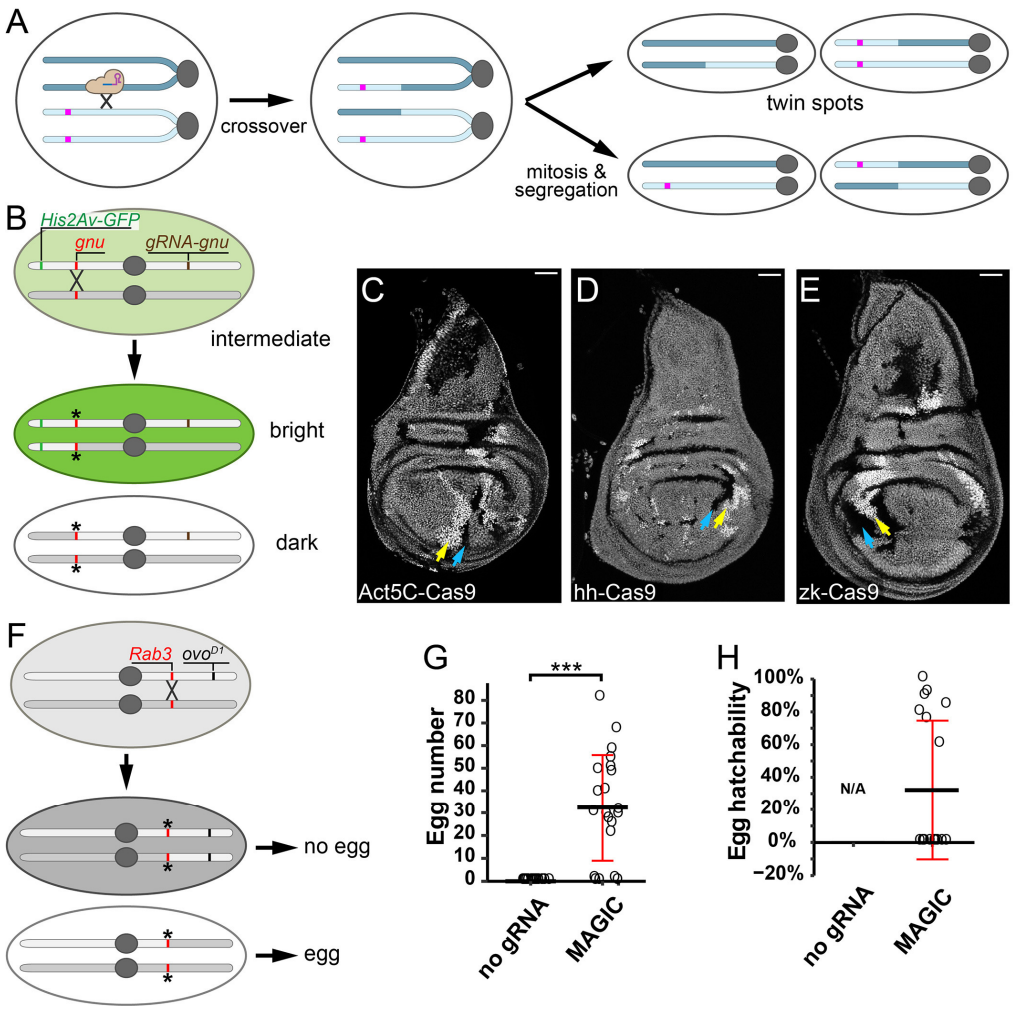

Figure 1. CRISPR-induced crossover generates somatic and germline clones in *Drosophila*

(A) A diagram illustrating how a CRISPR/Cas9-induced DSB leads to generation of homozygous clones in a heterozygous organism. The magenta bar indicates an allele that becomes homozygous in the twin spots.

(B) Strategy for generating mosaic clones using the *His2Av-GFP* marker and a crossover at the *gnu* locus.

(C-E) Mosaic clones in wing discs visualized by levels of *His2Av-GFP* expression, as described in the text. A pair of arrows indicate *His2Av-GFP*$^{+/+}$ (yellow) and *His2Av-GFP*$^{-/-}$ (blue) cells in each panel. Clones were induced by *Act5C-Cas9* (**C**), *hh-Cas9* (**D**) and *zk-Cas9* (**E**). Scale bars, 50 µm.

(F) Strategy for generating and detecting clones in the female germline using *ovo*^{D1}.

(G) Number of eggs produced by females carrying *nos-Cas9* and *ovo*^{D1}, with (MAGIC) or without (no gRNA) *gRNA-Rab3*. ***p<0.001, Student's t test. n=number females: no gRNA (n=18); MAGIC (n=18).

(H) Hatchability of eggs produced females carrying *nos-Cas9* and *ovo*^{D1}, with (MAGIC) or without (no gRNA) *gRNA-Rab3*. n=number females: no gRNA (N/A); MAGIC (n=18).

For all quantifications, black bar, mean; red bar, SD. Asterisks in (B) and (F) indicate mutated gRNA target sites.

84 populations of cells homozygous for the chromosome segment distal to the exchange.

85 ***Using CRISPR-induced crossover to generate clones in the* Drosophila *soma and germline***

86 For our initial tests of the ability of MAGIC to generate mosaic clones in somatic tissues, we used
87 ubiquitously expressed gRNAs to induce DSBs at the *gnu* locus and a ubiquitous fluorescent marker,
88 *His2Av-GFP* [32], to trace clones (Figure 1B). Both *His2Av-GFP* and *gnu* are located on the left arm of
89 chromosome 3 (3L), and *His2Av-GFP* is distal to *gnu*. We chose *gnu* as our gRNA target because we
90 have already made an efficient *gRNA-gnu* line for other purposes (to be published elsewhere);
91 furthermore, this gene is only required maternally for embryonic development [33], so mutations of *gnu*
92 are not expected to affect the viability or growth of somatic cells. We induced clones using three
93 different Cas9 transgenes, each of which is expressed in the developing wing disc under the control of
94 a different enhancer. With all three Cas9s, we observed twin spots consisting of bright *His2Av-GFP*
95 homozygous clones abutting GFP-negative clones in the midst of *His2Av-GFP/+* heterozygous cells
96 (Figures 1C-1E) in every imaginal disc examined, demonstrating the feasibility of MAGIC for generating
97 somatic mosaics.

98 Given that CRISPR/Cas9 is active in both the soma and the germline of *Drosophila* [34–36], we
99 next tested for MAGIC clone induction in the germline by using the DFS technique and the germline-
100 specific *nos-Cas9* [35] (Figure S1A). We used an ovo^{D1} transgene located on chromosome arm 2R and
101 induced DSBs at the *Rab3* locus, which is located on the same arm proximal to the location of ovo^{D1}
102 (Figure 1F). Since *Rab3* is a non-essential gene expressed only in neurons [37], its disruption in the
103 female germline should affect neither egg production nor embryonic development of the progeny. Due
104 to the dominant effect of ovo^{D1}, restoration of egg production can only result from mitotic recombination
105 proximal to ovo^{D1} (e.g. at *Rab3* in this case), followed by generation of ovo^{D1} negative clones. As
106 expected, control females that contained ovo^{D1} and *nos-Cas9*, but not *gRNA-Rab3*, did not produce any
107 eggs. In contrast, most females carrying all three components produced 20-90 eggs each (Figure 1G),
108 many of which hatched into larvae (Figure 1H), suggesting successful mitotic recombination.

109 The results above together show that, like the Flp/FRT system, MAGIC is an effective approach

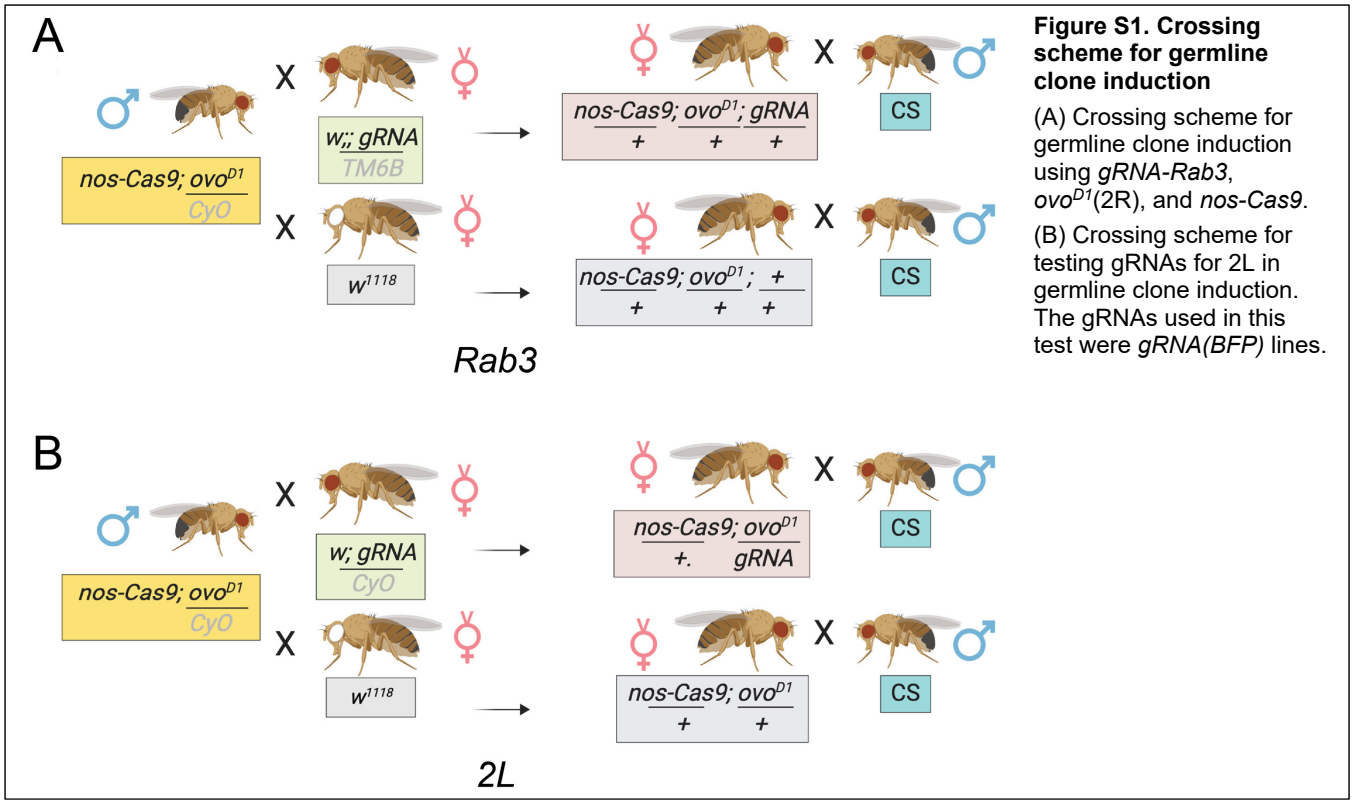

Figure S1. Crossing scheme for germline clone induction

(A) Crossing scheme for germline clone induction using *gRNA-Rab3*, *ovo*^{D1}(2R), and *nos-Cas9*.

(B) Crossing scheme for testing gRNAs for 2L in germline clone induction. The gRNAs used in this test were *gRNA(BFP)* lines.

for generating homozygous clones via mitotic recombination in both *Drosophila* soma and germline, consistent with the high frequency of CRISPR-induced exchange of chromosomal arms previously demonstrated in the *Drosophila* germline [29]

A toolkit for generating labeled clones for genes on chromosome arm 2L

Towards making MAGIC a general approach for analyzing *Drosophila* genes, we built a toolkit for genes located on chromosome arm 2L as a proof-of-principle. We designed transgenic constructs that each integrate two features simultaneously: ubiquitously-expressed gRNAs that target a pericentromeric region and a ubiquitously-expressed marker for labeling clones. The constructs were inserted into a distal position of 2L. When used together with an unmodified 2nd chromosome, they label clones homozygous for nearly the entirety of the unmodified arm either negatively or positively. Negative labeling in the nMAGIC option is achieved by expressing a nuclear blue fluorescent protein (nBFP) reporter such that clones homozygous for the unmodified arm lose nBFP expression (Figure 2A). Positive labeling with pMAGIC utilizes a Gal80 marker [17], which suppresses Gal4-driven expression of a fluorescent reporter (Figure 2B). Therefore, only the cells that lose Gal80 transgene will

be fluorescently labeled, similarly to mosaic analysis with a repressible cell marker (MARCM) [17].

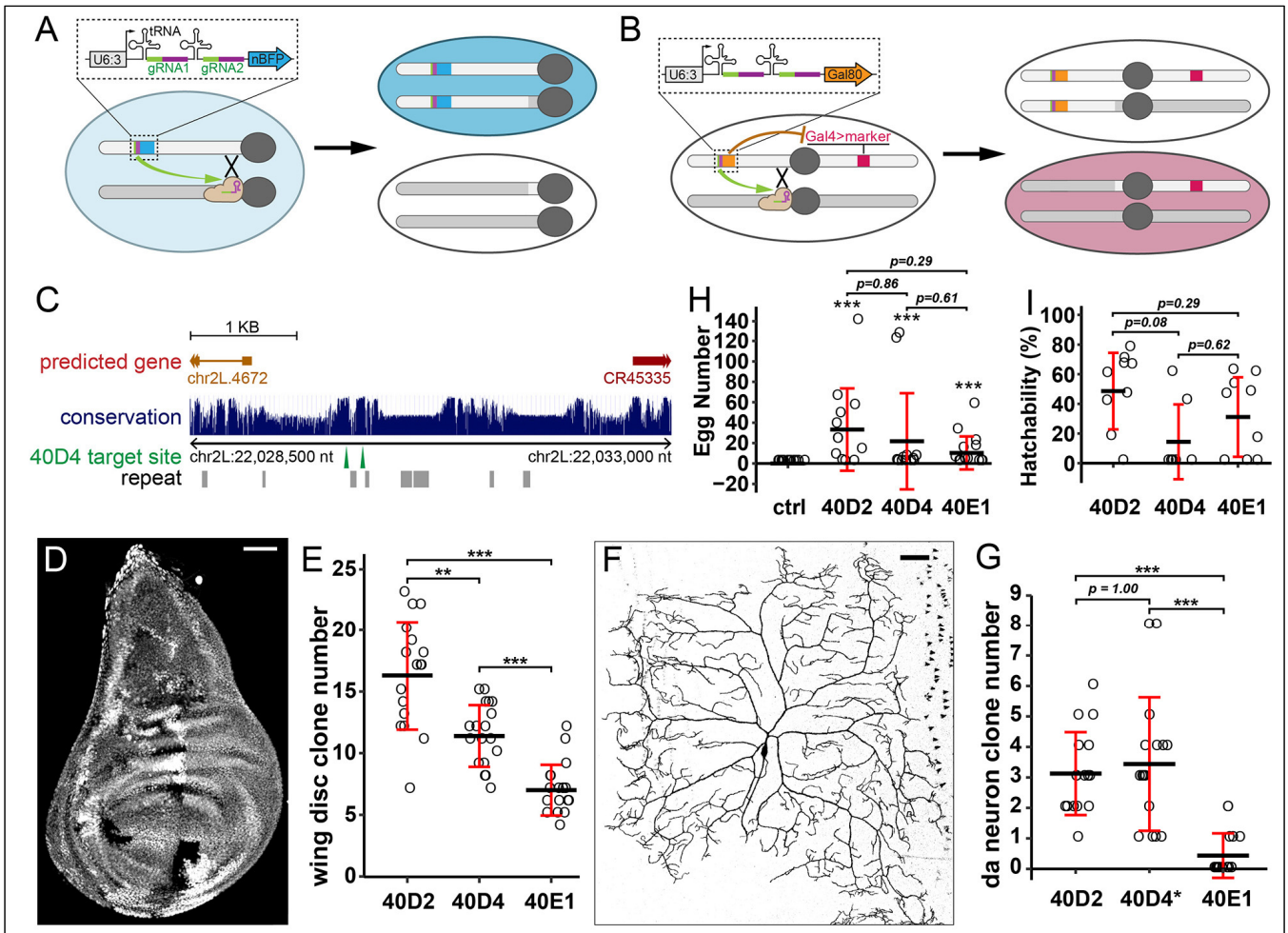

Figure 2. A toolkit for generating labeled clones for genes on chromosome arm 2L.

(A) Strategy for generating negatively labeled clones for genes on 2L using nuclear BFP.

(B) Strategy for generating positively labeled clones for genes on 2L using Gal80.

(C) A map for gRNA-(40D4) target sites derived from the UCSC Genome Browser. The height of the conservation bar corresponds to the level of conservation among 23 *Drosophila* species.

(D) A wing imaginal disc showing clones generated by a negative labeling construct (nBFP) paired with *hh-Cas9*.

(E) Number of clones in wing discs using three different gRNA(BFP) constructs. n=number of discs: 40D2 (n=17); 40D4 (n=18); 40E1(n=18). Welch's t-tests, p-values corrected using Bonferroni method; **p≤0.01, ***p≤0.001.

(F) A C4da neuron clone generated by a positive labeling construct (Gal80) paired with *SOP-Cas9* and *ppk>CD4-tdTom*.

(G) Quantification of C4da clones using three different gRNA(Gal80) constructs. n=number of larvae: 40D2 (n=16); 40D4 (n=16); 40E1 (n=16). Clones were visualized by *ppk>CD4-tdTom*. Welch's t-tests, p-values corrected using Bonferroni method; ***p≤0.001. The asterisk on 40D4 indicates frequent labeling of C3da clones.

(H) Number of eggs produced by using *ovo*^{D1}(2L), *nos-Cas9*, and three different gRNA(BFP) constructs. The control (ctrl) has no gRNA. n=number of females: ctrl (n=13); 40D2 (n =12); 40D4 (n=12); 40E1 (n=14). Asterisks are from *post hoc* single sample t-tests that compare the estimated marginal mean (EMM) of each gRNA against the control (μ = 0); ***p≤0.001. p-values are from contrasts of EMMs of each gRNA (excluding control). EMMs are based on a negative binomial model. All p-values were corrected using the Tukey method.

(I) Hatchability of eggs produced by females carrying *ovo*^{D1}(2L), *nos-Cas9*, and gRNA(BFP) constructs. n=number female: 40D2 (n=9); 40D4 (n=7); 40E1(n=9). p-values are from contrasts of EMMs of proportions of hatched/non-hatched eggs for each gRNA based on a binomial, mixed-effects model and were corrected using the Tukey method.

For all quantifications: black bar, mean; red bar, SD. Scale bars, 50 μm.

125 To identify appropriate gRNA target sites, we surveyed the pericentromeric sequences of 2L for
126 sequences that met three criteria: (1) being reasonably conserved so that DSBs can be induced in most
127 *Drosophila* strains; (2) not functionally critical and being distant from essential sequences so that indel
128 mutations in nearby regions would not disrupt important biological processes; and (3) unique in the
129 genome, so as to avoid off-target effects. Therefore, for each MAGIC construct, we chose a pair of non-
130 repeat gRNA target sequences in an intergenic region to enhance the chance of DSBs. The two gRNA
131 target sequences are closely-linked to reduce the risk of large deletions (Figure 2C). In addition, we
132 preferentially chose sequences that are conserved among closely related *Drosophila* species (*D.*
133 *melanogaster*, *D. simulans*, and *D. sechellia*) but not in more distant species. Considering the varying
134 efficiencies of different gRNA target sequences, we selected three pairs of gRNAs targeting three
135 chromosomal locations (40D2, 40D4, and 40E1) and tested their ability to produce clones in wing discs,
136 neurons, and the germline.

137 Clones were induced in a specific tissue by a Cas9 transgene that is expressed in precursor
138 cells of that tissue. We used *hh-Cas9* [38] for nMAGIC in the wing imaginal disc (Figure 2D), *SOP-Cas9*
139 [38] for pMAGIC in larval class IV dendritic arborization (C4da) sensory neurons (Figure 2F), and *nos-*
140 *Cas9* for the female germline (Figure S1B). gRNAs targeting 40D2 consistently performed the best in

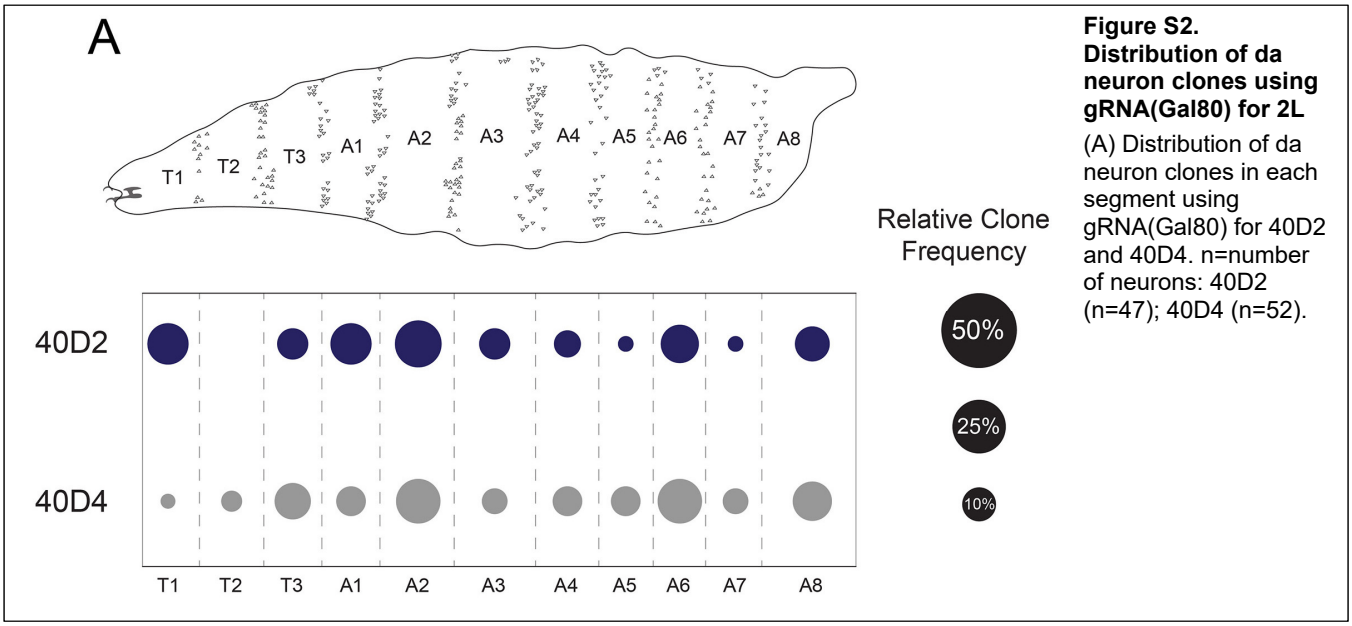

Figure S2. Distribution of da neuron clones using gRNA(Gal80) for 2L

(A) Distribution of da neuron clones in each segment using gRNA(Gal80) for 40D2 and 40D4. n=number of neurons: 40D2 (n=47); 40D4 (n=52).

generating clones in wing discs and C4da neurons (Figures 2E and 2G) and appear to be the most efficient in the germline, even though the differences in the germline were not statistically significant (Figures 2H and 2I). Although the overall efficiencies of *gRNA-40D2* and *gRNA-40D4* in inducing clones in da neurons are similar (Figure 2G and Figure S2A), *gRNA-40D4* induced more clones in a different type of neuron (class III). The fact that the three gRNA pairs showed similar trends in their ability to induce clones across different tissues suggests that an efficient gRNA construct for one tissue will likely perform well in other tissues also. These results indicate that we have created an efficient MAGIC toolkit for genes located on chromosome arm 2L. Analogous toolkits could easily be made for any other chromosome arm, using the same methods.

Clonal analysis of neuronal dendrite development

To evaluate the utility of our MAGIC toolkit for characterizing gene function at the single-cell level, we combined the pMAGIC line *gRNA-40D2(Gal80)* with mutations on 2L that affect dendrite morphogenesis in C4da neurons by disrupting vesicular trafficking. We first used two genes, *Secretory 5* (*Sec5*) [39] and *Rab5* [40], that have been shown to be required for dendrite growth. We observed dendrite reduction in C4da clones carrying homozygous mutations in these genes (Figures 3A and 3B), recapitulating previously published results using MARCM with the same mutants [39,40]. A third gene, *Syntaxin 5* (*Syx5*), was identified in our unpublished RNAi screens. Clones carrying a null mutation of *Syx5* produced the most dramatic dendrite reduction, with almost all terminal dendrites eliminated (Figure 3C), consistent with the expected role of Syx5 in ER to Golgi vesicle trafficking [41]. Therefore, our MAGIC reagents for 2L can be used to characterize gene functions in single cells with a power

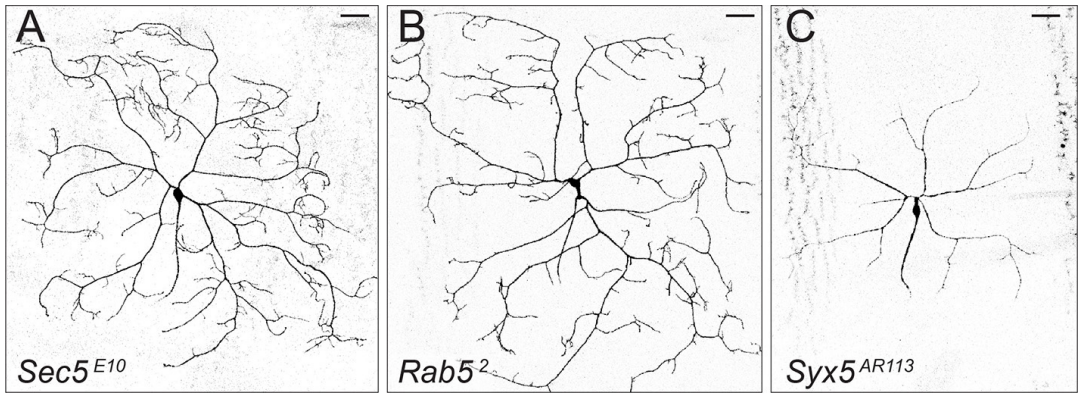

Figure 3. Clonal analysis of example genes in neuronal dendrite development

(A-C) MAGIC clones of C4da neurons using *Sec5*^{E10} (A), *Rab5*^{2} (B) and *Syx5*^{AR113} (C), visualized by *ppk>MApHS*. Scale bars, 50 μm.

161 analogous to that of MARCM but with a much simpler system.

162 ***Generation of clones by MAGIC in fly lines with wild-derived genomes***

163 A substantial advantage of MAGIC compared to Flp/FRT-based mitotic recombination systems is that
164 MAGIC does not require prior genetic modification of the chromosome arm to be tested. It therefore has
165 the potential to be applied to fly strains with wild-derived genomes, and even other organisms. To test
166 the applicability of MAGIC to unmarked strains with wild-derived genomes, we crossed *gRNA-*
167 *40D2(nBFP); hh-Cas9* to five randomly chosen lines from the *Drosophila* Genetic Reference Panel
168 (DGRP) [42], a set of standard strains established from flies captured in the wild. In all cases, we
169 observed efficient clone induction in wing imaginal discs (Figures 4A-4E), demonstrating the potential of
170 MAGIC for clonal analysis of the function of natural alleles residing on wild-derived chromosomes.

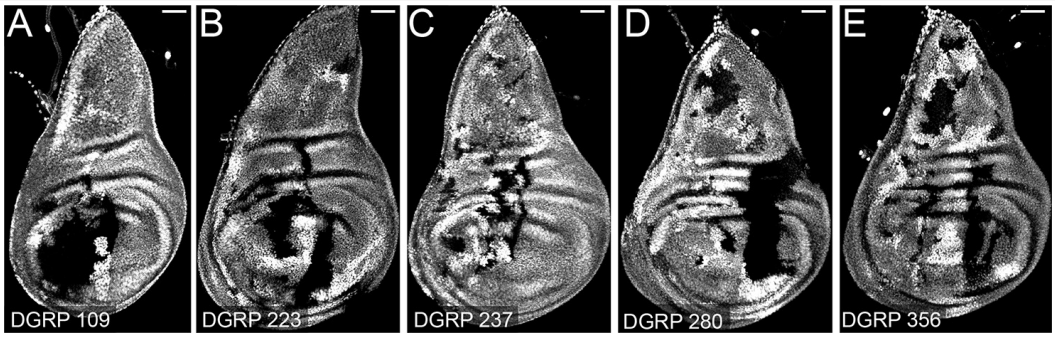

Figure 4. MAGIC generates clones with DGRP lines
(A-E) Clones in wing imaginal discs by pairing *gRNA-40D2(BFP); hh-Cas9* with DGRP line 109 (A), 223 (B), 237 (C), 280 (D) and 356 (E). Scale bars, 50 μm.

171 **Discussion:**

172 We present here a new technique we name MAGIC (mosaic analysis by gRNA-induced crossing-over)
173 for clonal analysis based on CRISPR-induced mitotic recombination. We show that MAGIC is capable
174 of producing efficiently mosaic tissues in both the *Drosophila* soma and germline, using gRNAs
175 targeting various chromosomal locations. Integrated gRNA-marker constructs enable both positive- and
176 negative-labeling of homozygous clones. As demonstrated by our 2L toolkit, MAGIC is simple and
177 effective to use; similar MAGIC reagents can be generated easily for all other chromosome arms to
178 allow for genome-wide characterization of gene functions.

179 Although conventional Flp/FRT-based techniques have been widely and successfully used in
180 *Drosophila* for similar clonal analyses [11], MAGIC has two major advantages. The first is the simplicity
181 of MAGIC assays: This system eliminates the requirement for genetic modification of the test

182 chromosome; furthermore, integrating gRNAs and genetic markers into one transgenic construct further
183 reduces the number of necessary genetic components. Therefore, gRNA-marker transgenes can be
184 combined with existing mutant libraries to perform MAGIC with very little additional effort. The second
185 advantage of MAGIC is that mitotic recombination is not limited by the available FRT insertion sites.
186 While introducing FRT to a specific pericentromeric region is very difficult and historically required
187 labor-intensive genetic screens, CRISPR/Cas9 can induce DNA DSBs and subsequent crossover at
188 specific pericentromeric sequences with ease. Therefore, MAGIC opens doors for clonal analysis of
189 genes that were previously impossible to study using existing FRT sites, such as those on the fourth
190 chromosome [29] and the ones near centromeres. In addition, many *Drosophila* mutations are
191 associated with transgenic constructs containing FRT [43], making analyses complicated when using
192 Flp/FRT-based techniques. In contrast, MAGIC should be compatible with all of these gene disruption
193 lines.

194 The unique mechanism of MAGIC requires three considerations for successful applications.
195 First, our results suggest that the gRNA target sequence strongly influences the efficiency of clone
196 induction, likely by affecting the frequency of DNA DSBs in premitotic cells. Therefore, for clonal
197 analysis of a specific chromosomal arm, it is beneficial to compare a few candidate gRNA targets and
198 select the most effective one. Second, because perfect DSB repair will recreate the gRNA target site
199 and allow for one more round of Cas9 cutting, most cells that have expressed Cas9 in their lineages
200 are expected to eventually harbor indel mutations that disrupt the gRNA target site, regardless of
201 whether or not the DSBs have led to mitotic recombination. However, this caveat can be mitigated by
202 choosing gRNA sites in non-critical sequences, which can be validated by crossing gRNA lines to a
203 ubiquitous Cas9 or by comparing gRNA-induced control clones to wildtype cells. Lastly, since only DNA
204 DSBs in the G_2 phase can lead to clone generation, the timing of Cas9 action is expected to be critical
205 for MAGIC. For the cell type in question, an ideal Cas9 should be expressed in the precursor cells, as
206 too early expression can mutate gRNA target sites prematurely and too late expression will lead to
207 unproductive DSBs.

208 Perhaps the most exciting aspect of MAGIC is its potential for use with wild-derived *Drosophila*
209 strains and in organisms beyond *Drosophila*. DGRP wild-derived strains have played important roles in
210 identification of natural alleles that are associated with certain phenotypic variations [44–47]. However,
211 it has been difficult to investigate the effect of homozygosity for alleles within these strains without
212 being able to use available genetic tools (e.g. Gal4 drivers and fluorescent markers) in *Drosophila*. By
213 combining MAGIC with the DGRP, it is now possible to validate causal effects of specific natural alleles
214 in cellular or developmental processes in a tissue-specific manner. The DGRP can also be used in
215 MAGIC-based genetic screens to identify natural alleles that, when made homozygous, can cause or
216 modify certain phenotypes. Importantly, MAGIC can in theory be utilized in a wide array of organisms
217 that are compatible with CRISPR/Cas9 [48]. In model systems that allow for transgenesis of gRNA-
218 marker constructs, such as mouse, zebrafish, and *Xenopus*, Cas9 can be introduced by injection or
219 virus transduction to further simplify genetic manipulations. Therefore, the flexibility and power of
220 mosaic analysis that are familiar to the *Drosophila* research community are now in reach of researchers
221 who study organisms which have not, or have rarely, been amenable to clonal analysis.

222 **Materials and Methods:**

223 ***Fly Stocks and Husbandry***

224 See the Key Resource Table for details of fly stocks used in this study. Broadly, all fly lines were either
225 generated in the Han and Wolfner labs, or obtained from the Bloomington *Drosophila* Stock Center or
226 the *Drosophila* Genetic Reference Panel [42]. All flies were grown on standard yeast-glucose medium,
227 in a 12:12 light/dark cycle, at room temperature (22 ± 1°C, for the egg laying assay) or 25°C (for larval
228 assays) unless otherwise noted. Virgin males and females for mating experiments were aged for 3-5
229 days. Virgin females were aged on yeasted food for germline clonal analysis.

230 To test germline clone induction, we combined *nos-Cas9* and ovo^{D1}, and then the gRNA in two
231 sequential crosses in schemes shown in Figure S1.

232 To visualize clones of C4da neurons, we used *ppk-Gal4 UAS-CD4-tdTom* (Figure 2) and *ppk-*
233 *Gal4 UAS-MApHS* (Figure 3, only the tdTom channel is shown).

234 ***Molecular Cloning***

235 *zk-Cas9:* The entry vector pENTR221-ZK2 [49] and the destination vector pDEST-APIC-Cas9
236 (Addgene 121657) were combined in a Gateway LR reaction to generate the expression vector
237 pAPIC2-ZK2-Cas9.

238 *MAGIC gRNA-marker vectors*: gRNA-marker vectors were constructed similarly to pAC-U63-tgRNA-
239 Rev (Addgene 112811, Poe et al., 2019) but have either a ubi-nBFP (in pAC-U63-tgRNA-nlsBFP) or a
240 ubi-Gal80 (in pAC-U63-tgRNA-Gal80) marker immediately after the U6 3' flanking sequence. The
241 markers contain a Ubi-p63E promoter, mTagBFP-NLS or Gal80 coding sequence, and His2Av polyA
242 sequence. The Ubi-p63E promoter was amplified from *Ubi-CasExpress* genomic DNA using the
243 oligonucleotides TTAATGCGTATGCATTCTAGTggccatggcttgctgttcttcgcgttc and
244 TTGGATTATTctgcgggcagaaaatagagatgtggaaaattag. mTagBFP-NLS was synthesized as a gBlock
245 DNA fragment (Integrated DNA Technologies, Inc.). Gal80 coding sequence was PCR amplified from
246 pBPGAL80Uw-4 (Addgene 26235) using the oligonucleotides
247 aaaaaaaaatcaaaATGAGCGGTACCGATTACAACAAAAGGAGTAGTGTGAG and
248 GCCGACTGGCTTAGTTAattaattctagaTTAAAGCGAGTAGTGGGAGATGTTG. The His2Av polyA
249 sequence was PCR amplified from pDEST-APLO (Addgene 112805). DNA fragments were assembled
250 together using NEBuilder DNA Assembly (New England Biolabs Inc.).

251 *gRNA expression vectors:* For *gnu* and *Rab3*, gRNA target sequences were cloned into pAC-U63-
252 tgRNA-Rev as described [38]. For gRNAs targeting 2L, gRNA target sequences were cloned into pAC-
253 U63-tgRNA-nlsBFP and pAC-U63-tgRNA-Gal80 using NEBuilder DNA Assembly. In the gRNA-marker
254 constructs, the tRNA between the first and second gRNAs is a *Drosophila* glutamine tRNA
255 (cagcgcGGTTCCATGGTGTAATGGTTAGCACTCAGGACTCTGAATCCTGCGATCCGAGTTCAAATCT
256 CGGTGGAACCT) instead of a rice glycine tRNA.

257 Injections were carried out by Rainbow Transgenic Flies (Camarillo, CA 93012 USA) to
258 transform flies through φC31 integrase-mediated integration into attP docker sites.
259 pAPIC2-ZK2-Cas9 and gRNA-marker constructs were integrated into the *attP*^{VK00037} site on the second

260 chromosome and expression vectors containing gRNAs targeting *Rab3* or *gnu* were integrated into the
261 *attP*^{VK00027} site on the third chromosome. Transgenic insertions were validated by genomic PCR or
262 sequencing.

263 ***Identification of gRNA target sequence***

264 gRNA target sequences for *Rab3* and *gnu* were identified as described previously [38]. Briefly, two
265 gRNA prediction methods were used: sgRNA Scorer 2.0 [50]
266 (https://crispr.med.harvard.edu) and Benchling (www.benchling.com). Candidate target sequences
267 were those that obtained high on-target scores in both algorithms. CasFinder [51] was used to identify
268 and reject any sequences with more than one target site. Two target sequences against coding exons
269 for all splice isoforms were chosen for each targeted gene. gRNA target sequences for 2L were
270 identified by visually scanning through pericentromeric sequences using UCSC Genome Browser
271 (https://genome.ucsc.edu/) following principles described in the Results section. The gRNA target
272 sequences are listed in the table below.

Gene	**Target sequence 1**	**Target sequence 2**
gnu	TTCGAATGTAAAAGCTTCGG	TTCCTGCCAACGCCTCCAGT
Rab3	GCCCACCGTGGAGACGAAGG	AGTGCGACATGGAGGACCAG
40D2	AGTCACCTGAAATAAGTCAG	GTTAGCCATCACAAGAACAG
40D4	GGGTTGTCTCCTGATATGGG	AACCGAACTGAACTCAACTG
40E1	CCGAATGATTTCATGTGAAG	TAGGGCAATTAAATATGTCA

273 ***Live Imaging of neurons***

274 Live imaging was performed as previously described [49]. Briefly, animals were reared at 25˚C in
275 density-controlled vials for between 96 and 120 hours after egg-laying (to obtain third to late-third instar
276 larvae). Larvae were mounted in glycerol and their C4da neurons at segments A1-A6 were imaged
277 using a Leica SP8 confocal microscope with a 20x oil objective and a z-step size of 3.5 μm.

278 ***Imaginal disc imaging***

279 Imaginal disc dissections were performed as described previously [52]. Briefly, wandering third instar
280 larvae were dissected in a small petri dish filled with cold PBS. The anterior half of the larva was
281 inverted and the trachea and gut were removed. The sample was then transferred to 4% formaldehyde
282 in PBS and fixed for 15 minutes at room temperature. After washing with PBS, the imaginal discs were
283 placed in SlowFade Diamond Antifade Mountant (Thermo Fisher Scientific) on a glass slide. A coverslip
284 was lightly pressed on top. Imaginal discs were imaged using a Leica SP8 confocal microscope with a
285 20X oil objective.

286 ***Assays for Germline Clonal Analysis***

287 To monitor mitotic recombination events resulting in germline clone generation, we performed egg-
288 laying and egg hatchability assays as detailed in Hu and Wolfner (2019), with the exception of using
289 Canton-S males in place of ORP2 males as wild-type mates. Hatchability was calculated only for
290 females that laid eggs. Females that laid no eggs were eliminated from hatchability calculations to
291 avoid inflation of false-zero values.

292 ***Image Analysis and Quantification***

293 Counting of wing disc clones was completed manually in Fiji/ImageJ. Counting of neuronal clones was
294 completed manually during the imaging process.

295 ***Statistical Analysis***

296 Statistical analyses were performed in R. Student's t-test was conducted for egg-laying data using *Rab*
297 and *kni* gRNAs. For egg-laying data using the 2L toolkit, we performed estimated marginal means
298 contrasts between gRNAs and *post hoc* one sample t-tests using a generalized linear model with a
299 negative binomial response. For hatchability data using the 2L toolkit, we performed estimated marginal
300 means contrasts between proportions of hatched/non-hatched eggs for each gRNA using a generalized
301 linear mixed-effects model with a binomial response. For all contrasts, p-values were corrected for
302 multiple comparisons using the Tukey method. For wing disc and neuronal clone data, we performed
303 Welch's analysis of variance (ANOVA) followed by pairwise *post hoc* Welch's t-tests. p-values from the
304 multiple *post hoc* Welch's t-tests were corrected for multiple comparisons using the Bonferroni method.

Acknowledgments:

We thank Bloomington *Drosophila* Stock Center (NIH P40OD018537) and the *Drosophila* Genetic Reference Panel for fly stocks; Cedric Feschotte, Andy Clark, Eric Alani, and Marcus Smolka for advice on gRNA design; Cornell CSCU consultants Stephen Parry and Erika Mudrak for advice on statistics; Michael Goldberg, John Schimenti, Erich Brunner, and Konrad Basler for critical reading and suggestions on the manuscript. This work was supported by a Cornell start-up fund and NIH grants (R01NS099125 and R21OD023824) awarded to C.H., an NIH grant (R01-HD038921) awarded to M.W., and an NIH training grant (T32-GM07273) awarded to the Cornell BMCB graduate program that supported S.A.

References:

1. Perrimon N. Creating mosaics in Drosophila. Int J Dev Biol. 1998;42: 243–247. doi:10.1387/ijdb.9654004
2. Garcia-Bellido A, Ripoll P, Morata G. Developmental compartmentalization in the dorsal mesothoracic disc of Drosophila. Dev Biol. 1976;48: 132–147. doi:10.1016/0012-1606(76)90052-X
3. Heitzler P, Simpson P. The choice of cell fate in the epidermis of Drosophila. Cell. 1991;64: 1083–1092. doi:10.1016/0092-8674(91)90263-X
4. Perrimon N, Engstromt L, Mahowald AP. Zygotic Lethals With Specific Maternal Effect Phenotypes in Drosophila melanogaster. I. Loci on the X Chromosome. Genetics. 1989;121: 333–352.
5. Feng Y, Irvine KD. Fat and Expanded act in parallel to regulate growth through Warts. PNAS. 2007;104: 20362–20367. doi:10.1073/pnas.0706722105
6. Huang X, Shi L, Cao J, He F, Li R, Zhang Y, et al. The Sterile 20-Like kinase tao controls tissue homeostasis by regulating the hippo pathway in drosophila adult midgut. J Genet Genomics. 2014;41: 429–438. doi:10.1016/j.jgg.2014.05.007
7. Chung BY, Ro J, Hutter SA, Miller KM, Guduguntla LS, Kondo S, et al. Drosophila Neuropeptide

331 F Signaling Independently Regulates Feeding and Sleep-Wake Behavior. Cell Rep. 2017;19:
332 2441–2450. doi:10.1016/j.celrep.2017.05.085
333 8. Hu DJ-K, Jasper H. Control of Intestinal Cell Fate by Dynamic Mitotic Spindle Repositioning
334 Influences Epithelial Homeostasis and Longevity. Cell Rep. 2019;28: 2807-2823.e5.
335 doi:10.1016/j.celrep.2019.08.014
336 9. Lee T. Generating mosaics for lineage analysis in flies. Wiley Interdiscip Rev Dev Biol. 2014;3:
337 69–81. doi:10.1002/wdev.122
338 10. Stern C. Somatic Crossing Over and Segregation In Drosophlia melanogaster. Genetics.
339 1936;21: 625–730.
340 11. Griffin R, Binari R, Perrimon N. Genetic odyssey to generate marked clones in Drosophila
341 mosaics. PNAS. 2014;111: 4756–4763. doi:10.1073/pnas.1403218111
342 12. Muller HJ. The Production of Mutations by X-Rays. PNAS. 1928;14: 714–726.
343 13. Xu T, Rubin G. The effort to make mosaic analysis a household tool. Development. 2012;139:
344 4501–1503. doi:10.1242/dev.085183
345 14. Golic KG, Lindquist S. The FLP recombinase of yeast catalyzes site-specific recombination in the
346 drosophila genome. Cell. 1989;59: 499–509. doi:10.1016/0092-8674(89)90033-0
347 15. Xu T, Rubin G. Analysis of genetic mosaics in developing and adult Drosophila tissues.
348 Development. 1993;117: 1223–1237.
349 16. Harrison DA, Perrimon N. Simple and efficient generation of marked clones in Drosophila. Curr
350 Biol. 1993;3: 424–433.
351 17. Lee T, Luo L. Mosaic Analysis with a Repressible Neurotechnique Cell Marker for Studies of
352 Gene Function in Neuronal Morphogenesis. Neuron. 1999;22: 451–461.
353 18. Yu H-H, Chen C-H, Shi L, Huang Y, Lee T. Twin-spot MARCM to reveal the developmental origin
354 and identity of neurons. Nat Neurosci. 2009;12. doi:10.1038/nn.2345
355 19. Griffin R, Sustar A, Bonvin M, Binari R, Del Valle Rodriguez A, Hohl AM, et al. The twin spot
356 generator for differential Drosophila lineage analysis. Nat Methods. 2009;6: 600–602.

357 doi:10.1038/NMETH.1349
358 20. Perrimon N, Gans M. Clonal analysis of the tissue specificity of recessive female-sterile
359 mutations of Drosophila melanogaster using a dominant female-sterile mutation Fs(1)K1237.
360 Dev Biol. 1983;100: 365–373. doi:10.1016/0012-1606(83)90231-2
361 21. Chou T-B, Perrimon N. Use of a Yeast Sitespecific Recombinase to Produce Female Germline
362 Chimeras in Drosophila. Genetics. 1992;131: 643–653.
363 22. Chou T-B, Noll E, Perrimon N. Autosomal P[ovoD1] dominant female-sterile insertions in
364 Drosophila and their use in generating germ-line chimeras. Development. 1993;119: 1359–1369.
365 23. Zong H, Espinosa, J S, Su HH, Muzumdar MD, Luo L. Mosaic Analysis with Double Markers in
366 Mice. Cell. 2005;121: 479–492.
367 24. Henner A, Ventura PB, Jiang Y, Zong H. MADM-ML, a Mouse Genetic Mosaic System with
368 Increased Clonal Efficiency. PLoS One. 2013;8: 77672. doi:10.1371/journal.pone.0077672
369 25. Sander JD, Keith Joung J. CRISPR-Cas systems for editing, regulating and targeting genomes.
370 Nat Biotechnol. 2014;32: 347–355. doi:10.1038/nbt.2842
371 26. Jinek M, Chylinski K, Fonfara I, Hauer M, Doudna JA, Charpentier E. A Programmable Dual-
372 RNA-Guided DNA Endonuclease in Adaptive Bacterial Immunity. Science (80-). 2012;337: 816–
373 821. Available: http://science.sciencemag.org/
374 27. Salsman J, Dellaire G. Precision genome editing in the CRISPR era. Biochem Cell Biol. 2017;95:
375 187–102. doi:10.1139/bcb-2016-0137
376 28. Sadhu MJ, Bloom JS, Day L, Kruglyak L. CRISPR-directed mitotic recombination enables
377 genetic mapping without crosses. Science (80-). 2016;352: 1113–1116. Available:
378 http://science.sciencemag.org/
379 29. Brunner E, Yagi R, Debrunner M, Beck-Schneider D, Burger A, Escher E, et al. CRISPR-induced
380 double-strand breaks trigger recombination between homologous chromosome arms. Life Sci
381 Alliance. 2019;2: e201800267. doi:10.26508/lsa.201800267
382 30. Heinze SD, Kohlbrenner T, Ippolito D, Meccariello A, Burger A, Mosimann C, et al. CRISPR-

383 Cas9 targeted disruption of the yellow ortholog in the housefly identifies the brown body locus.
384 Sci Rep. 2017;7. doi:10.1038/s41598-017-04686-6
385 31. Hayut SF, Melamed Bessudo C, Levy AA. Targeted recombination between homologous
386 chromosomes for precise breeding in tomato. Nat Commun. 2017;8. doi:10.1038/ncomms15605
387 32. Clarkson M, Saint R. A His2AvDGFP Fusion Gene Complements a Lethal His2AvD Mutant Allele
388 and Provides an in Vivo Marker for Drosophila Chromosome Behavior. DNA Cell Biol. 1999;18:
389 457–462. Available: www.liebertpub.com
390 33. Freeman M, Niisslein-Volhard C, Glover' DM. The Dissociation of Nuclear and Centrosomal
391 Division in gnu, a Mutation Causing Giant Nuclei in Drosophila. Cell. 1966.
392 34. Gratz SJ, Cummings AM, Nguyen JN, Hamm DC, Donohue LK, Harrison MM, et al. Genome
393 Engineering of Drosophila with the CRISPR RNA-Guided Cas9 Nuclease. Genetics. 2013;194:
394 1029–1035. doi:10.1534/genetics.113.152710
395 35. Port F, Chen H-M, Lee T, Bullock SL. Optimized CRISPR/Cas tools for efficient germline and
396 somatic genome engineering in Drosophila. PNAS. 2014;111: E2967–E2976.
397 doi:10.1073/pnas.1405500111
398 36. Ren X, Sun J, Housden BE, Hu Y, Roesel C, Lin S, et al. Optimized gene editing technology for
399 Drosophila melanogaster using germ line-specific Cas9. PNAS. 2013;110: 19012–19017.
400 doi:10.1073/pnas.1318481110
401 37. Chen S, Gendelman HK, Roche JP, Alsharif P, Graf ER. Mutational Analysis of Rab3 Function
402 for Controlling Active Zone Protein Composition at the Drosophila Neuromuscular Junction.
403 PLoS One. 2015;10: e0136938. doi:10.1371/journal.pone.0136938
404 38. Poe AR, Wang B, Sapar ML, Ji H, Li K, Onabajo T, et al. Mutagenesis Reveals Gene
405 Redundancy and Perdurance in Drosophila. Genetics. 2019;211: 459–472.
406 39. Peng Y, Lee J, Rowland K, Wen Y, Hua H, Carlson N, et al. Regulation of dendrite growth and
407 maintenance by exocytosis. J Cell Sci. 2015;128: 4279–4292. doi:10.1242/jcs.174771
408 40. Satoh D, Sato D, Tsuyama T, Saito M, Ohkura H, Rolls MM, et al. Spatial control of branching

409 within dendritic arbors by dynein-dependent transport of Rab5-endosomes. Nat Cell Biol.
410 2008;10: 1164–1171. doi:10.1038/ncb1776
411 41. Hardwick KG, Pelham HRB. SED5 encodes a 39-kD integral membrane protein required for
412 vesicular transport between the ER and the Golgi complex. J Cell Biol. 1992;119: 513–521.
413 doi:10.1083/jcb.119.3.513
414 42. MacKay TFC, Richards S, Stone EA, Barbadilla A, Ayroles JF, Zhu D, et al. The Drosophila
415 melanogaster Genetic Reference Panel. Nature. 2012;482: 173–178. doi:10.1038/nature10811
416 43. Thibault ST, Singer MA, Miyazaki WY, Milash B, Dompe NA, Singh CM, et al. A complementary
417 transposon tool kit for Drosophila melanogaster using P and piggyBac. Nat Genet. 2004;36:
418 283–287. doi:10.1038/ng1314
419 44. Grenier JK, Arguello JR, Moreira MC, Gottipati S, Mohammed J, Hackett SR, et al. Global
420 Diversity Lines-A Five-Continent Reference Panel of Sequenced Drosophila melanogaster
421 Strains. G3 Genes Genomes Genet. 2015;5: 593–603. doi:10.1534/g3.114.015883
422 45. Clark AG, Silveriat S, Meyerst W, Langleyt CH. Nature screen: An efficient method for screening
423 natural populations of Drosophila for targeted P-element insertions (transposon tagging/reverse
424 genetics/PCR/mutagenesis). Genetics. 1994;91: 719–722.
425 46. Mackay TFC, Huang W. Charting the genotype-phenotype map: lessons from the Drosophila
426 melanogaster Genetic Reference Panel. Wiley Interdiscip Rev Dev Biol. 2018;7: e289.
427 doi:10.1002/wdev.289
428 47. Shorter J, Couch C, Huang W, Carbone MA, Peiffer J, Anholt RRH, et al. Genetic architecture of
429 natural variation in Drosophila melanogaster aggressive behavior. PNAS. 2015; E3555–E3563.
430 doi:10.1073/pnas.1510104112
431 48. Harrison MM, Jenkins B V, O'connor-Giles KM, Wildonger J. A CRISPR view of development.
432 Genes Dev. 2014;28: 1859–1872. doi:10.1101/gad.248252.114
433 49. Poe AR, Tang L, Wang B, Li Y, Sapar ML, Han C. Dendritic space-filling requires a neuronal
434 type-specific extracellular permissive signal in Drosophila. PNAS. 2017; E8062–E8071.

435 doi:10.1073/pnas.1707467114

436 50. Chari R, Yeo NC, Chavez A, Church GM. SgRNA Scorer 2.0: A Species-Independent Model to
437 Predict CRISPR/Cas9 Activity. ACS Synth Biol. 2017;6: 902–904.
438 doi:10.1021/acssynbio.6b00343

439 51. Aach J, Mali P, Church GM. CasFinder: Flexible algorithm for identifying specific Cas9 targets in
440 genomes. bioRxiv. Cold Spring Harbor Laboratory; 2014 May. doi:10.1101/005074

441 52. Han C, Belenkaya TY, Wang B, Lin X. Drosophila glypicans control the cell-to-cell movement of
442 Hedgehog by a dynamin-independent process. Development. 2004;131: 601–611.
443 doi:10.1242/dev.00958

444 53. Hu Q, Wolfner MF. The Drosophila Trpm channel mediates calcium influx during egg activation.
445 PNAS. 2019;116: 18994–19000. doi:10.1073/pnas.1906967116

446

Key Resource Table

REAGENT or RESOURCE	SOURCE	IDENTIFIER	ADDITIONAL INFORMATION
Experimental Models: Organisms/Strains			
ppk-Gal4	Han et al., 2012		*ppk-Gal4* ^{VK00037}
ppk-Gal4	Han et al., 2012		*ppk-Gal4* ^{1A}
UAS-CD4-tdTom	Han et al., 2011	RRID:BDSC_35841	*UAS-CD4-tdTom* ^{7M1}
UAS-MApHS	Han et al., 2014		*UAS-MApHS* ^{VK00019}
His2Av-GFP	Bloomington Drosophila Stock Center	RRID:BDSC_5941	*His2Av-GFP(S65T)* ^{62A}
Act5C-Cas9	Bloomington Drosophila Stock Center	RRID:BDSC_54590	*Act5C-Cas9.P*
hh-Cas9	Poe et al., 2019		*R28E04-Cas9* ^{6A}
SOP-Cas9	Poe et al., 2019		*[sc-E1]x8-Cas9* ^{3A}
zk-Cas9	This study		*zk-Cas9* ^{VK00037}
nos-Cas9	Bloomington Drosophila Stock Center	RRID:BDSC_54591	*nos-Cas9.P* $^{ZH-2A}$
ovo ^{D1} *2L*	Bloomington Drosophila Stock Center	RRID:BDSC_2121	*ovoD1-18* ^{2La} *ovoD1-18* ^{2Lb}
ovo ^{D1} *2R*	Bloomington Drosophila Stock Center	RRID:BDSC_4434	*ovoD1-18* ^{2R}
gRNA-gnu	This study		*gRNA-gnu(U63)* ^{VK00027}
gRNA-Rab3	This study		*gRNA-Rab3* ^{VK00027}
gRNA-40D2(BFP)	This study		*w; gRNA-40D2(BFP)* ^{VK00037}
gRNA-40D4(BFP)	This study		*w; gRNA-40D4(BFP)* ^{VK00037}
gRNA-40E1(BFP)	This study		*w; gRNA-40E1(BFP)* ^{VK00037}
40D2(Gal80)	This study		*w; gRNA-40D2(Gal80)* ^{VK00037}
40D4(Gal80)	This study		*w; gRNA-40D4(Gal80)* ^{VK00037}
gRNA-40E1(Gal80)	This study		*w; gRNA-40E1(Gal80)* ^{VK00037}
gRNA-40D2(BFP)	This study		*w; gRNA-40D2(BFP)* ^{VK00037}
gRNA-40D4(BFP)	This study		*w; gRNA-40D4(BFP)* ^{VK00037}
Rab5 ^{2}	Bloomington Drosophila Stock Center	RRID:BDSC_42702	
Sec5 ^{E10}	Bloomington Drosophila Stock Center	RRID:BDSC_81044	
Syx5 ^{AR113}	Bloomington Drosophila Stock Center	RRID:BDSC_3645	
DGRP 109	Mackay et al., 2012	RRID:BDSC_28140	
DGRP 223	Mackay et al., 2012		
DGRP 237	Mackay et al., 2012		
DGRP 280	Mackay et al., 2012	RRID:BDSC_28164	
DGRP 356	Mackay et al., 2012	RRID:BDSC_28178	
Recombinant DNA			
pENTR221-ZK2	Poe et al., 2017		
pDEST-APIC-Cas9	Poe et al., 2019	RRID:Addgene_121657	
pAC-U63-tgRNA-Rev	Poe et al., 2019	RRID:Addgene_112811	
Ubi-CasExpress ^{attP40}	Bloomington Drosophila Stock Center	RRID:BDSC_65419	Genomic DNA used as a PCR template
pBPGAL80Uw-4	Addgene	RRID: Addgene_26235	
pDEST-APLO	Poe et al., 2017	RRID: Addgene_112805	

Key Resource Table

Software and Algorithms			
Fiji	https://fiji.sc/	RRID: SCR_002285	
R	https://www.r-project.org/	RRID: SCR_001905	
Adobe Photoshop	Adobe	RRID:SCR_014199	
Adobe Illustrator	Adobe	RRID:SCR_010279	
Other			
Gateway™ LR Clonase™ II Enzyme mix	Thermo Fisher Scientific,	#11791020	
NEBuilder® HiFi DNA Assembly Master Mix	New England Biolabs Inc.	#E2621	